NANO LETTERS

Letter

pubs.acs.org/NanoLett

High-Curvature Nanostructuring Enhances Probe Display for Biomolecular Detection

Phil De Luna,[†] Sahar S. Mahshid,[‡] Jagotamoy Das,[‡] Binquan Luan,[†] Edward H. Sargent,[§] Shana O. Kelley,*[,‡,⊥] and Ruhong Zhou*[,†,¶,∥]

[†]Computational Biology Center, IBM Thomas J. Watson Research Center, Yorktown Heights, New York 10598, United States

[‡]Department of Pharmaceutical Sciences, Leslie Dan Faculty of Pharmacy, [§]Department of Electrical and Computer Engineering, Faculty of Engineering, and [⊥]Department of Biochemistry, Faculty of Medicine, University of Toronto, Toronto, Ontario M5S 3M2, Canada

[¶]Institute of Quantitative Biology and Medicine, SRMP and RAD-X, Collaborative Innovation Center of Radiological Medicine of Jiangsu Higher Education Institutions, Soochow University, Suzhou 215123, China

[∥]Department of Chemistry, Columbia University, New York, New York 10027, United States

Supporting Information

ABSTRACT: High-curvature electrodes facilitate rapid and sensitive detection of a broad class of molecular analytes. These sensors have reached detection limits not attained using bulk macroscale materials. It has been proposed that immobilized DNA probes are displayed at a high deflection angle on the sensor surface, which allows greater accessibility and more efficient hybridization. Here we report the first use of all-atom molecular dynamics simulations coupled with electrochemical experiments to explore the dynamics of single-stranded DNA immobilized on high-curvature versus flat surfaces. We find that high-curvature structures suppress DNA probe aggregation among adjacent probes. This results in conformations that are more freely accessed by target molecules. The effect observed is amplified in the presence of highly charged cations commonly used in electrochemical biosensing. The results of the simulations agree with experiments that measure the degree of hybridization in the presence of mono-, di-, and trivalent cations. On high-curvature structures, hybridization current density increases as positive charge increases, whereas on flat electrodes, the trivalent cations cause aggregation due to electrostatic overscreening, which leads to decreased current density and less sensitive detection.

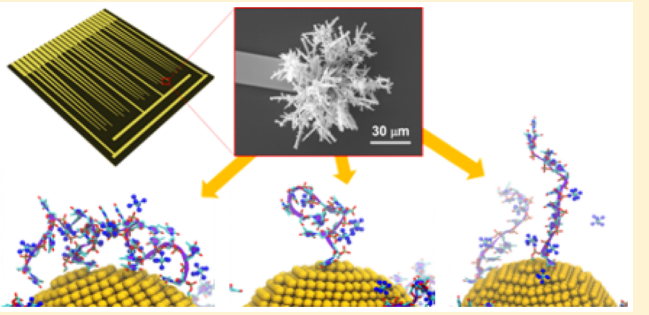

KEYWORDS: *Molecular dynamics, biosensing, DNA hybridization, nanostructured microelectrodes, high-curvature effects*

Rapid and portable diagnostic tests administered close to the point-of-care are of interest for physician offices, hospitals, rural clinics, and in remote locations in the developing world. Ultrasensitive and low-cost biomolecular detection has been achieved in recent years due to advances in devices based on electrochemical detection.[1−13] Several platforms have been successfully applied in the detection of nucleic acids, small molecules, and even protein targets, and in the best cases, these systems achieved attomolar detection levels.[14−20]

One highly sensitive detection approach relies on the hybridization of surface-immobilized single-stranded DNA (ssDNA) probe molecules to complementary target sequences. Once the captured strands have hybridized, electrochemical reporter groups, that can be either covalently[21−23] or electrostatically bound,[24−30] produce an electrochemical signal (Figure 1b) proportional to the amount of target bound.[31]

In these systems, efficient hybridization can be limited by steric probe−probe interactions and high probe densities on flat electrodes that hinder target binding. Nanostructured microelectrodes (NMEs; Figure 1a) address this problem by using high-curvature morphologies to overcome kinetic penalties associated with dense probe packing.[18,32] These structures have achieved large molecular-to-electrical signal amplification,[33] and this system has been used in the detection of cancer biomarkers,[19] infectious pathogens,[34] and in organ transplant assessment.[20]

Two hypotheses have been offered to explain why high-curvature electrodes exhibit such high selectivity and hybridization efficiency. In the first, they are proposed to provide higher surface areas, which allow for a greater number of probes and hybridization sites. In the second, it has been proposed that nanostructuring promotes the display and accessibility of probe molecules by increasing their deflection angle, which allows for more space between probes for efficient hybridization.[15,18,35]

Received: December 12, 2016
Revised: January 10, 2017
Published: January 11, 2017

ACS Publications © XXXX American Chemical Society

DOI: 10.1021/acs.nanolett.6b05153
Nano Lett. XXXX, XXX, XXX−XXX

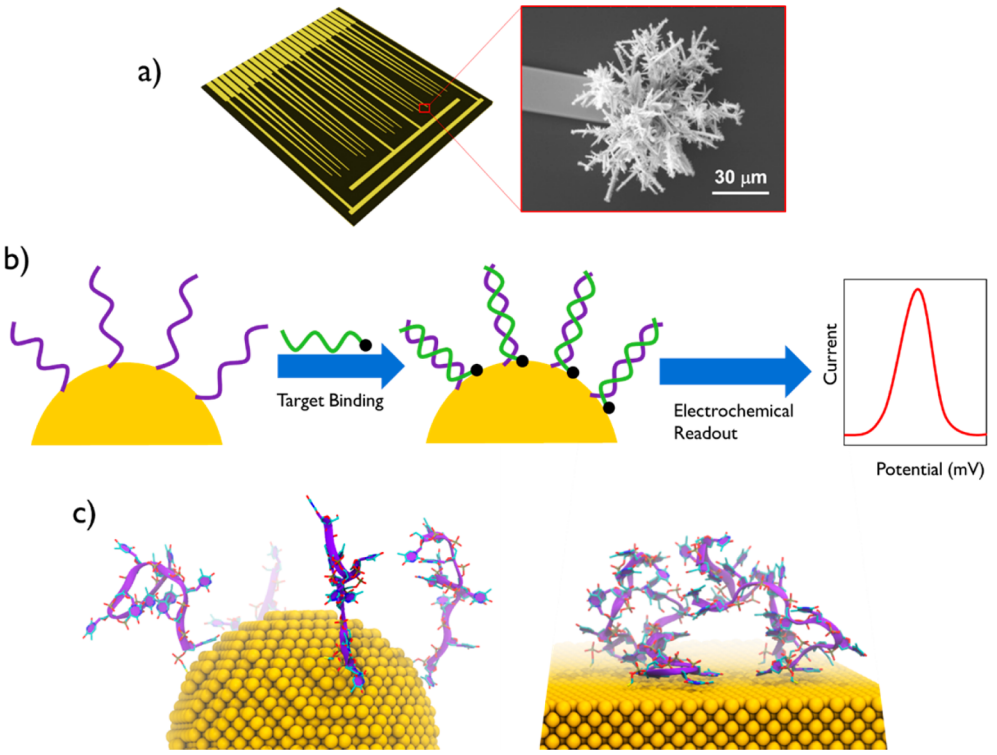

Figure 1. (a) Integrated circuit (left) patterned with gold leads and nanostructured microelectrodes (NMEs) with an SEM image close up of a NME (right). (b) Schematic of a representative electrochemical biodetection assay in which probes are first exposed to target molecules that hybridize. Next, the duplexes are exposed to a redox reporter, which produces an electrochemical current directly related to the number of bound target molecules. (c) Molecular dynamics snapshots of high-curvature surfaces with greater probe accessibility (left) and flat surfaces with a higher degree of probe aggregation (right).

Secondary effects offered include that a large surface area of sharp structures protruding into solution could be utilized to promote interactions between biomolecule targets and probes.[36] Furthermore, NMEs benefit from increased transport of redox reporters via radial diffusion at the high-curvature tips, which allow for amplified electrochemical currents.[17]

We believed that simple static models such as these offer an approximate view of how increases in biosensing efficiency and sensitivity could be achieved using finely nanostructured electrodes and that a more physically accurate and detailed model was worth developing, one that would look at the dynamic nature of probes on flat versus high-curvature nanostructures.

Kinetic and thermodynamic mechanisms that influence hybridization of target molecules to DNA probes have been previously investigated, both via theory and experiment. An electrostatic model that optimized the hybridization density on planar surfaces as a function of DNA surface density, salt concentrations, and applied voltages was developed and validated experimentally.[37] Furthermore, an experimental and theoretical approach was used to study the hybridization thermodynamics on high-curvature gold nanoparticles with high probe coverages. Coarse-grained molecular dynamics revealed that at higher probe loadings there is an increased enthalpic penalty to DNA hybridization due to an increase in surface charge density.[38] These studies projected hybridization efficiencies that approached 100%. In parallel investigations, it was found that the hybridization of free DNA is governed by an electrostatic barrier due to (i) the accumulation of negative charges as target molecules bind and (ii) by conformational changes at distal sites induced by subsequent binding events.[38]

The presence of salt is another essential component needed for DNA hybridization with standard protocols using NaCl buffer concentrations in the hundreds of millimolar or Mg^{2+} cation concentrations in the tens of millimolar range.[39] The addition of cations is necessary to stabilize the negatively charged phosphate groups in the backbone of the DNA molecules[40] and is an important factor which directly impacts probe-target hybridization. Similarly, coarse grained molecular dynamics simulations have been used to study the crystallization of spherical nucleic acid (SNA)−gold nanoparticle conjugates driven by DNA hybridization.[41] High loadings of negatively charged probes on the surface require more cations to shield and stabilize the compact negative charges.[42]

Herein, we sought to quantify and compare atomic-level probe dynamics on the surfaces of flat and high-curvature surfaces. We used explicit solvent, all-atom, molecular dynamics simulations to study ssDNA probes on planar and high-curvature gold surfaces to elucidate the relationship of probe accessibility with curvature. To study the difference in electrostatic effects between flat and high-curvature surfaces, we performed simulations with mono-, di-, and trivalent cations. For mono- and divalent cations, we chose Na^+ and Mg^{2+}, which are standard salts used in many buffer solutions for DNA-based applications.[39,40] For the highly charged trivalent cation, we chose to focus on $[Ru(NH_3)_6]^{3+}$ (hereafter referred to as Ru^{3+}), a common redox reporter used in many electrochemical biosensing assays.[43,44] Simulations suggest that the electrostatic effects of Ru^{3+} are much more prominent in comparison to monovalent Na^+ or divalent Mg^{2+}. In fact, the interactions of Ru^{3+} lead to probe aggregation due to increased probe−probe entanglement at high concentrations. This

DOI: 10.1021/acs.nanolett.6b05153
Nano Lett. XXXX, XXX, XXX−XXX

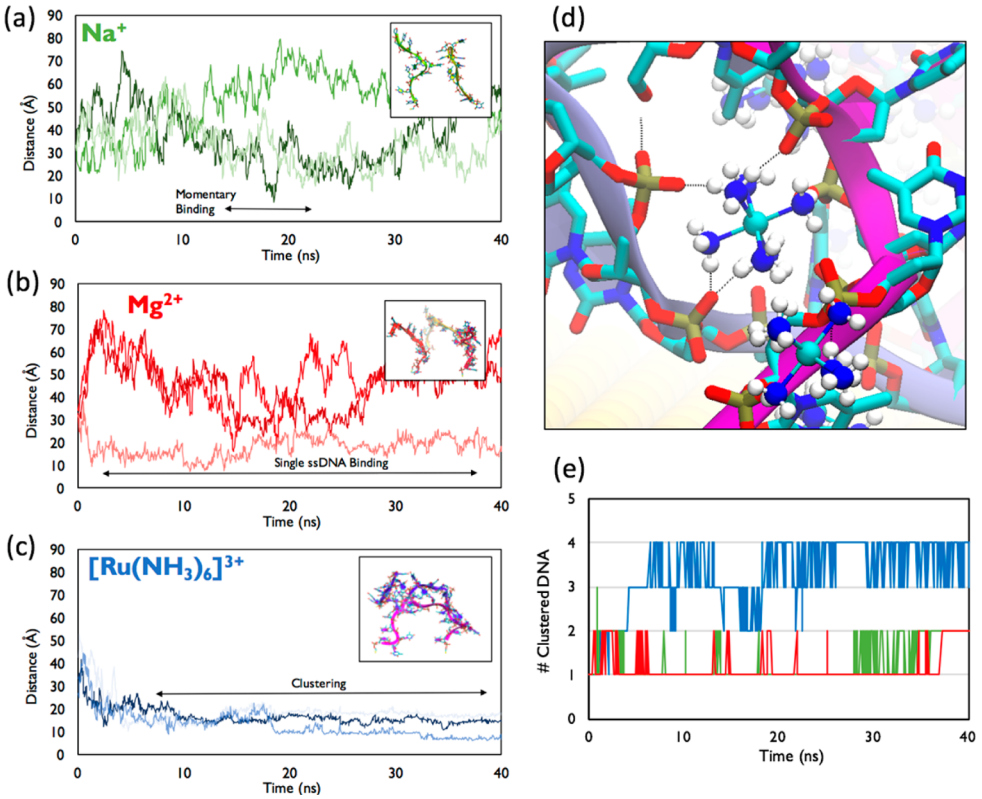

Figure 2. Calculated ssDNA−ssDNA distances versus time between one strand and three adjacent strands (light, medium, and dark colored) in the presence of (a) Na^+, (b) Mg^{2+}, and (c) Ru^{3+}. The trivalent cations induce ssDNA aggregation into clusters, whereas the mono- and divalent cations do not. Snapshots of ssDNA interactions in last frame in the 40 ns simulation are also shown. (d) Zoom in of a Ru^{3+} cation bridging between two ssDNA strands depicted with dark blue and purple ribbons. (e) Number of clustered DNA over the 40 ns simulation in the presence of Na^+ (green), Mg^{2+} (red), and Ru^{3+} (blue).

aggregation is detrimental to hybridization and biosensing since the aggregation of adjacent probes renders it unavailable for target capture. We find that the degree of aggregation is, for each cation choice, substantially greater on flat surfaces than on high-curvature structures. We then performed experiments and found that as cation valency increases, hybridization also increases if NMEs are used as electrodes. In contrast, hybridization decreases on flat electrodes with cations possessing higher charges, which is in agreement with our theoretical predictions. Our findings suggest that the high-curvature NMEs promote efficient hybridization through suppression of probe aggregation and that the latter increases probe availability.

The goal of this study was to assess computationally whether probe molecules immobilized on flat surfaces versus those with nanoscale curvature exhibited conformational differences. We performed simulations of flat and high curvature surfaces in aqueous solutions containing Na^+, Mg^{2+}, and Ru^{3+}. We hypothesized that if significant probe−probe interaction effects existed for the different types of surfaces, they would be enhanced in the presence of more positively charged cations due to the charge screening effects. To experimentally test this hypothesis, we systematically varied solution conditions and measured hybridization induced currents to validate computational results.

We initiated the study with a set of MD simulations (computational details in the Supporting Information) focused on ssDNA immobilized on flat electrodes and found that interactions between ssDNA probes increase significantly as positive cation charge increased. We chose a fixed probe loading of ∼1 molecule/10 nm^2, which closely matched the optimal experimental probe surface coverage (10×10^{12} molecules/cm^2) for DNA hybridization efficiency.[18] Figure 2a−c show the ssDNA−ssDNA distance between the terminal phosphates of adjacent ssDNA strands on a flat gold surface in the presence of Na^+, Mg^{2+}, and Ru^{3+} cations. When Na^+ is present within solution, the ssDNA remains relatively linear and experiences transient binding interactions with adjacent strands. These interactions last 3−4 ns but do not persist throughout the analysis window. With divalent Mg^{2+}, we found that ssDNA may bind to another single adjacent strand and remain bound for the duration of the simulation, but typically there are no more than two interacting ssDNA strands at a time. Interestingly, in the presence of trivalent Ru^{3+}, it was found that the ssDNA probes aggregate into clusters of four strands or more within only 5 ns and remain bound for the remainder of the simulation (Figure 2e). ssDNA strands were considered in a cluster if they were within a 5 Å distance from an adjacent strand. Moreover, the Ru^{3+} cations all immediately bound to the negatively charged phosphate backbone of the ssDNA strands. In contrast, Na^+ and Mg^{2+} were more diffuse with cations interacting with the phosphate backbone and then returning to the bulk solvent. The Ru^{3+} cation acts as electrostatic bridge, which overcomes the repulsive interactions between two negatively charged ssDNA strands. Figure 2d shows that a large trivalent Ru^{3+} cation acts as a "glue" holding the ssDNA probes together and promoting the aggregation of the strands on the Au surface. Each equilibration run was

DOI: 10.1021/acs.nanolett.6b05153
Nano Lett. XXXX, XXX, XXX−XXX

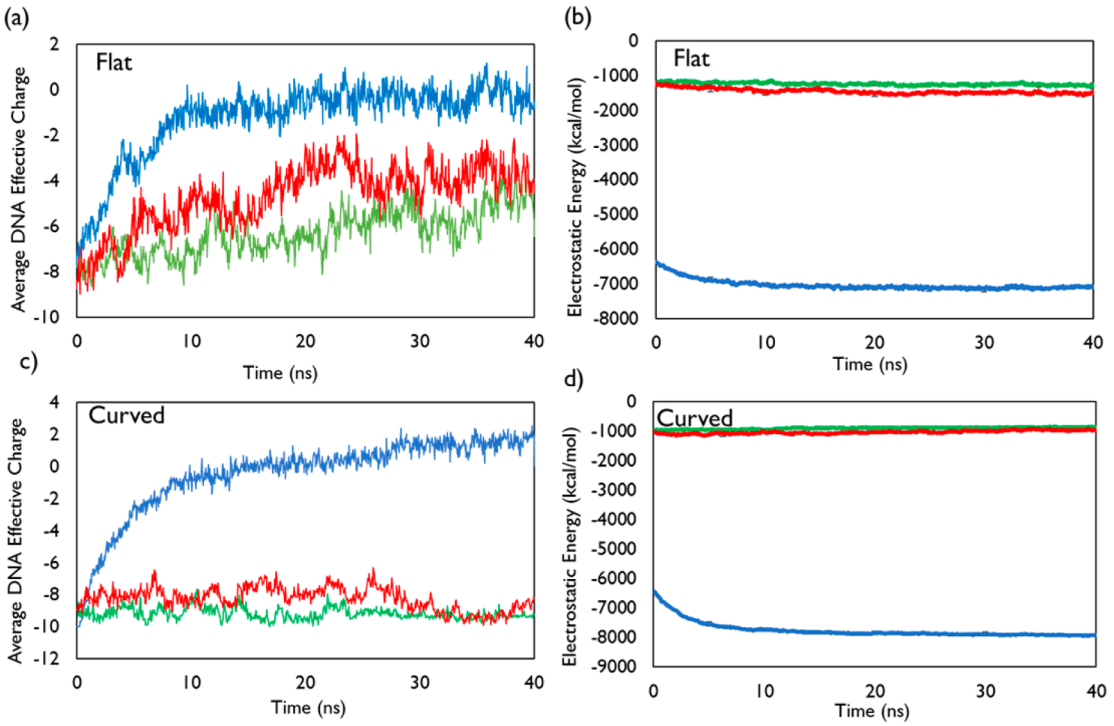

Figure 3. Average local effective charge per ssDNA strand on (a) a flat gold surface and (c) high curvature gold NP in the presence of Na^+ (green), Mg^{2+}(red), and Ru^{3+} (blue). The electrostatic energy per ssDNA strand on (b) a flat gold surface and (d) high curvature gold NP in the presence of Na^+ (green), Mg^{2+} (red), and Ru^{3+} (blue).

performed three times, for each cation, and the results remained consistent between various trials (Table S4).

To quantify the electrostatic effects that different cation charges had on ssDNA aggregation, we calculated the effective charge per ssDNA strand over the simulation as well as the electrostatic contribution to the total energy. The effective charge is defined as the sum of the average charge from bound cations and the charge of one ssDNA strand. On the gold surface, the average effective ssDNA charge per strand was found to approach zero after 10 ns in the presence of Ru^{3+}. This indicates that all trivalent cations bind to the phosphate backbone, thus providing sufficient electrostatic screening to cancel the repulsion between negatively charged ssDNA strands (Figure 3a). In contrast, in the presence of Na^+ and Mg^{2+}, the effective charge per ssDNA strand equilibrates to approximately −6e and −4e (where e is the charge of a proton), respectively, which indicates that the electrostatic repulsion between adjacent ssDNA strands is still present. The effective charge of a bare ssDNA is −9e due to the nine negatively charged phosphate groups per ssDNA. Next, we compared the electrostatic energies per strand in the presence of Na^+, Mg^{2+}, and Ru^{3+} (Figure 3b). Interestingly, it was found that the average electrostatic energies of Na^+ and Mg^{2+} were relatively similar (~1400 kcal/mol) despite Mg^{2+} being double the positive charge of Na^+. However, Ru^{3+} was found to have an electrostatic contribution 4.5-times larger than that of Na^+ or Mg^{2+}, which indicated that Ru^{3+} has a large energetic impact on the system. The electrostatic contributions were by far the largest contributions constituting 85%, 86%, and 89% of the total energy for Na^+, Mg^{2+}, and Ru^{3+} respectively.

Next, we sought to measure the dynamic movement of the cations at the probe/water interface. The average root−mean−square deviation (RMSD) was calculated for all cations over three independent simulations on a flat Au surface and is shown in Figure S5. For both Na^+ and Mg^{2+}, it was found that the RMSD increases rapidly until it converges within 3.25 ns to approximately 60 Å. In contrast, the RMSD of Ru^{3+} converges much quicker within only 1.5 ns to approximately 45 Å. This rapid convergence suggests that Ru^{3+} cations moved to their equilibrium position, which is bound to the ssDNA, much more rapidly than Na^+ or Mg^{2+}. As Na^+ is the lightest cation, one would expect the diffusion to be much greater than Ru^{3+}, which is a much heavier metal ion complex. Indeed, the calculated diffusion coefficients for Na^+, Mg^{2+}, and Ru^{3+} over the 40 ns simulation were found to be 3.94×10^{-4} cm^2/s, 3.71×10^{-4} cm^2/s, and 2.42×10^{-4} cm^2/s, respectively. These results reaffirm our findings that larger and more highly charged cations are less diffuse because they immediately bind to the backbone of ssDNA.

To compare the cation-influenced ssDNA aggregation present on high-curvature surfaces, we executed MD simulations for varying choices of cation, again with ssDNA on a 5.3 nm in diameter gold nanoparticle (Figure 3c,d). A histogram of ssDNA length, calculated as the distance between the terminal phosphor atoms, is shown in Figure S6. The average rise per base in the presence of Na^+ was found to be 2.5 Å ± 0.4 Å over the last 10 ns of the simulation. This result is consistent with previous molecular dynamics simulations on 2 nm gold nanoparticles, which found that in the presence of sodium cations ssDNA exhibited a 2.2 Å rise per base.[45] In contrast, the Mg^{2+} and Ru^{3+} had much a smaller rise per base at 1.9 Å ± 0.3 and 1.5 Å ± 0.1 Å, which indicated a more compressed strand structure.

We reconfirmed the trend that high cation charge promotes ssDNA aggregation, a trend that continues to hold true for surfaces with nanoscale curvature, but to a lesser extent than in the planar case. The slightly lower surface coverage of ssDNA on the NP is ~1 ssDNA/11 nm^2 with larger spacing between

DOI: 10.1021/acs.nanolett.6b05153
Nano Lett. XXXX, XXX, XXX−XXX

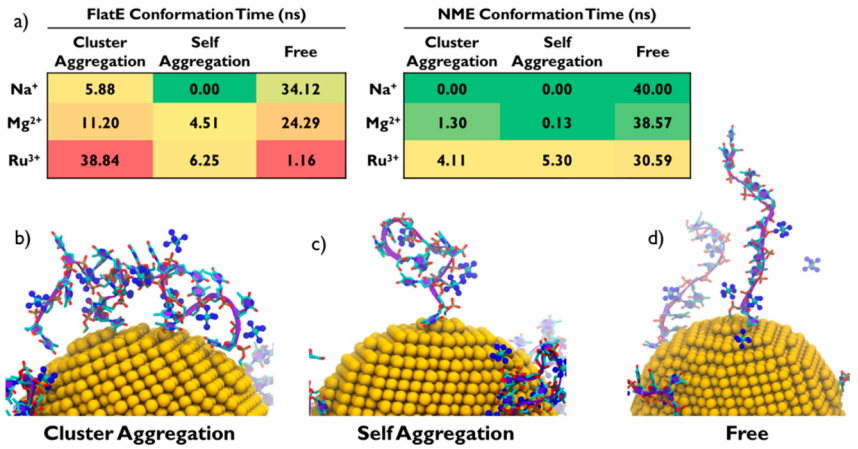

Figure 4. (a) Conformation time (ns) for flat and NME structures for Na^+, Mg^{2+}, and Ru^{3+} as a function of clustered aggregation, self-aggregation, and free. Green indicates more probe accessibility, while red indicates aggregation. (b) A snapshot of two adjacent ssDNA clustered together, these two strands remained interacting for the remainder of the simulation time. (c) Snapshot of a ssDNA curled up on itself in a self-aggregation conformation. (d) Snapshot of a ssDNA in a free conformation fully displayed and accessible.

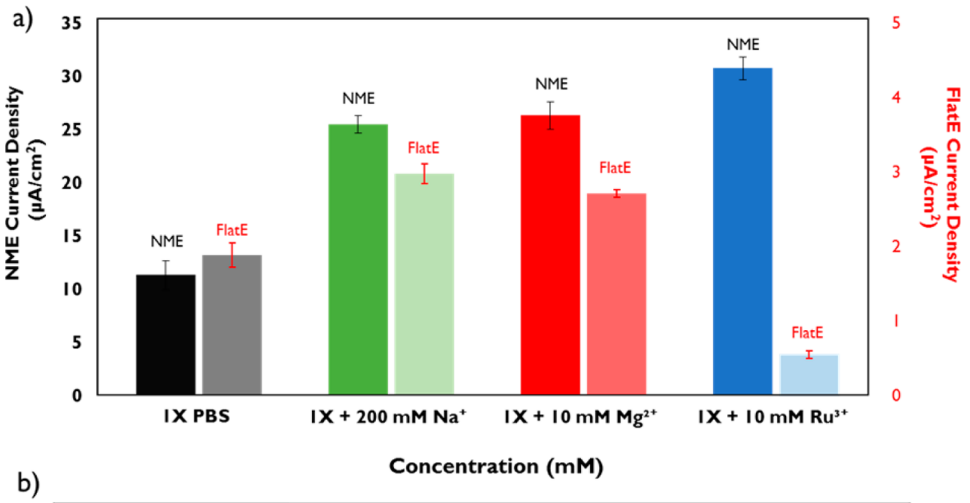

b)

	Na^+		Mg^{2+}		Ru^{3+}	
	Flat	NME	Flat	NME	Flat	NME
Maximum Current (μA)	0.835	0.013	0.864	0.013	0.237	0.017
Concentraiton (mM)	350	350	20	10	0.01	1

Figure 5. (a) Current density following hybridization in 1X PBS (150 mM NaCl) and added 200 mM Na^+, 10 mM Mg^{2+}, and 10 mM Ru^{3+} on high-curvature NMEs (left bar, left *y*-axis) and flat planar electrodes (right bar, right *y*-axis). (b) The maximum current among various tested concentrations of cations Na^+, Mg^{2+}, and Ru^{3+} added to 1X PBS solution from Figure S1.

adjacent strands and a greater deflection angle between probes compared to the flat gold surface (~1 ssDNA/10 nm^2). However, it was found that Ru^{3+} still has a significant impact on ssDNA aggregation. The ssDNA molecules tended to not interact with neighbors on the curved surfaces, but instead curled around the Ru^{3+} cation, thereby decreasing their probe length (Figure 4c). This is consistent with the experimental observation of unperturbed ssDNA mushroom conformations at low density regimes.[46] Moreover, select ssDNA strands were still capable of binding with another adjacent strand and forming an aggregate pair on the surface of the gold NP. In contrast, in the presence of Mg^{2+}, the ssDNA strands can momentarily interact but do not bind and Na^+ surrounding the negatively charged ssDNA results in no binding between strands at all. The average electrostatic energy over 3 runs was also similar to that found in the planar model where the electrostatic energy is approximately eight-times greater with Ru^{3+} than Mg^{2+} or Na^+ (Figure 3d). Furthermore, the average effective charge of DNA in the presence of Mg^{2+} and Na^+ on high curvature surfaces was found to be approximately −9e, which is more negatively charged than Mg^{2+} (−5e) and Na^+ (−6e) on flat surfaces. This suggests the charge screening effects of cations, which lead to probe aggregation, are suppressed on the high curvature surfaces.

Next, we sought to compare and quantify the degree of aggregation between flat and high-curvature surfaces. To this end, we have calculated the aggregation time of DNA as a function of cation for flat and NME structures. We classified three conformation states (cluster-aggregation, self-aggregation, and free), which served as descriptors for probe accessibility. Cluster-aggregation is defined as the time where two or more adjacent ssDNA molecules are within 5 Å of each other (Figure

DOI: 10.1021/acs.nanolett.6b05153
Nano Lett. XXXX, XXX, XXX−XXX

4b). Self-aggregation is when the ssDNA has curled onto itself and is defined as the time where the distance between a terminal phosphate group of a ssDNA and the gold surface is less than 30 Å, which is less than half the maximum outstretched length of a 10mer ssDNA molecule (Figure 4c). The probe is defined as free when it is not within 5 Å of an adjacent probe and when the $phosphate_{terminal}$ − gold distance is greater than 30 Å. The free state is calculated by subtracting the time of the two other aggregation states from the total 40 ns simulation time. A summary of the conformation times is visually shown in Figure 4a. As can be seen, the degree of aggregation increases for both flat electrode and NME with the longest aggregation time being 38.84 ns with Ru^{3+} on the flat electrode. It was found that the high-curvature surface suppresses aggregation as most of the simulation time the probes were in the free and accessible conformational state. In the case of Na^+ on the NME, there was absolutely no clustering or self-aggregation at all during the 40 ns run. The time scale sampled herein is far shorter than in reality; however, the trends of probe aggregation between flat and high-curvature surfaces remain.

Motivated by these intriguing theoretical predictions, we sought to investigate experimentally whether high-curvature NMEs suppressed probe aggregation and thus promoted efficient hybridization. Thus, we constructed a set of experiments to measure the hybridization efficiency on flat and high-curvature gold electrodes in the presence of Na^+, Mg^{2+}, and Ru^{3+} cations. To the best of our knowledge, this is the first time that use of trivalent cations for DNA hybridization has been studied. Electrochemical measurements were performed on planar gold electrodes and high-curvature gold NMEs with fixed immobilized probe loadings. Methylene blue covalently linked to a target sequence was used as the redox label in these experiments to independently assess the effects of electrostatically bound cations. Upon target and probe hybridization, the amount of methylene blue at the electrode surface increases. When methylene blue is reduced at the surface, a current signal is generated that reports on hybridization efficiency for the target molecule. Figure 5a shows the current density in $\mu A/cm^2$ as a function of cations. 1X PBS buffer (150 mM NaCl) was used as the baseline for experiments. Cations were then added to 1X PBS to yield solutions of 350 mM Na^+, 150 mM Na^+ + 10 mM Mg^{2+}, and 150 mM Na^+ + 10 mM Ru^{3+}. We chose to use 10 mM as the concentration for divalent and trivalent cations because it has been previously shown that the optimal concentration of Mg^{2+} for hybridization is within 10−15 mM.[40]

On planar electrodes, the current density was found to increase to 3 $\mu A/cm^2$ with the addition of 200 mM Na^+ to 1X PBS, which is in agreement with previous experimental results showing an increase of hybridization efficiency with DNA immobilized on gold at higher NaCl concentrations.[42] The current density with an addition of 10 mM Mg^{2+} to 1X PBS is slightly lower at 2.7 $\mu A/cm^2$ but reasonably similar to that of NaCl, which is consistent with previous work.[40] Interestingly, the current density is much lower with the addition of 10 mM Ru^{3+} at only 0.56 $\mu A/cm^2$ corresponding to an approximately four-fold decrease in current density. These results suggest that the hybridization is less efficient with the addition of Ru^{3+} on a flat planar electrode, which is in agreement with our theoretical predictions. The decrease in current density can be attributed to a greater degree of probe aggregation in the presence of the highly charged trivalent Ru^{3+}.

In stark contrast, the high-curvature nanostructured microelectrodes showed an opposite trend where the current density increased with respect to cation charge. The current densities for the NMEs were consistently far greater than on the flat planar electrode. The control 1X PBS had a current density of 11 $\mu A/cm^2$ on the NME and 2 $\mu A/cm^2$ on the flat electrode. The current density was found to increase with respect to cation valency on the NME rising to 26 $\mu A/cm^2$, 27 $\mu A/cm^2$, and 31 $\mu A/cm^2$ for added Na^+, Mg^{2+}, and Ru^{3+} respectively. The higher current density on the NME for Ru^{3+} compared to Mg^{2+} may arise from the fact that Ru^{3+}, in its capability as a redox reporter,[47] may contribute to the current in a manner that is additive to the methylene blue reporter bound to hybridized DNA. We also measured the hybridization induced current with respect to cation concentration of Na^+, Mg^{2+}, and Ru^{3+} (Figure S1). For the monovalent cation, the current increased with respect to concentration up to 350 mM. With higher charged divalent and trivalent cations, it was found that the current would increase until a certain concentration threshold, after which the current would decrease. This is because for higher concentrations the trivalent and divalent cations cause probe aggregation, which leads to a decrease in current. The maximum current attained at an optimal cation concentration is shown in Figure 5b. These results also match our molecular dynamics simulations and point toward increased activity of NMEs due to suppression of probe aggregation on the surface of the electrode.

In this work, the DNA aggregation and hybridization inhibition induced by highly charged cations were predicted using molecular dynamics simulations on flat and high-curvature surfaces and then experimentally investigated using an electrochemical assay. Molecular dynamics simulations showed that in the presence of Na^+, ssDNA probes were elongated and the probes were fully displayed for DNA hybridization; on Mg^{2+}, the probes may temporarily bind to each other but overall were available for hybridization; and with Ru^{3+}, the ssDNA probes would aggregate into clusters and remain unavailable for hybridization. It was found that highly curved surfaces quantitatively exhibited less probe aggregation in comparison to flat surfaces, and this effect was amplified in the presence of highly charged cations. This finding was then experimentally verified by measuring the current density as a function of cations on flat and high-curvature surfaces. This work implies that high concentrations of trivalent cations may limit sensing capabilities by reducing probe availability on flat surfaces. It elucidates the overscreening and probe aggregation effects that highly charged cations have on flat electrodes. Finally, it provides evidence that NMEs help to suppress probe aggregation by providing a complementary explanation to the increased deflection angle for the improvement in electrochemical signal. Thus, the insights reported here provide a deeper understanding of probe aggregation and DNA hybridization, which have far reaching implications in DNA self-assembly and may guide the future development and accelerate the design of materials used in a wide range of biomolecule sensors.

■ ASSOCIATED CONTENT

Supporting Information

The Supporting Information is available free of charge on the ACS Publications website at DOI: 10.1021/acs.nanolett.6b05153.

DOI: 10.1021/acs.nanolett.6b05153
Nano Lett. XXXX, XXX, XXX−XXX

Experimental methods; sequences of DNA strands; buffer solutions; electrochemical current measurements; computational methods; initial configuration of solvated Au slab and Au NP; initial starting model of $Ru(NH_6)^{3+}$ and Cl; plot of average Ru−N bond length; average RMSD of Na^+, Mg^{2+}, and Ru^{3+}; histogram of DNA length; nonbonded and bonded parameters for $[Ru(NH_3)_6]^{3+}$; plots of ssDNA−ssDNA distances (PDF)

AUTHOR INFORMATION

Corresponding Authors

*E-mail: ruhongz@us.ibm.com.

*E-mail: shana.kelley@utoronto.ca.

ORCID

Shana O. Kelley: 0000-0003-3360-5359

Ruhong Zhou: 0000-0001-8624-5591

Present Address

P.D.L., Department of Material Science and Engineering, Faculty of Engineering, University of Toronto, Toronto, Ontario M5S 3M2, Canada.

Author Contributions

The manuscript was written through contributions of all authors. All authors have given approval to the final version of the manuscript.

Notes

The authors declare no competing financial interest.

ACKNOWLEDGMENTS

P.D.L. is grateful to the Natural Sciences and Engineering Research Council of Canada (NSERC) for a Canadian Graduate Scholar−Doctoral (CGS-D) Scholarship and the IBM Research Internship program for financial support. P.D.L. is especially grateful to the members of the IBM TJ Watson Computational Biology Center for their mentorship and advice. This work is partially supported by the National Natural Science Foundation of China under Grant Nos. 11374221, 11574224, and 21320102003. R.Z. acknowledges the support from IBM Blue Gene Science Program (W125859, W1464125, and W1464164).

REFERENCES

(1) Kelley, S. O.; Mirkin, C. A.; Walt, D. R.; Ismagilov, R. F.; Toner, M.; Sargent, E. H. *Nat. Nanotechnol.* **2014**, *9* (12), 969.

(2) Xiao, Y.; Qu, X.; Plaxco, K. W.; Heeger, A. J. *J. Am. Chem. Soc.* **2007**, *129* (39), 11896.

(3) Patolsky, F.; Weizmann, Y.; Willner, I. *J. Am. Chem. Soc.* **2002**, *124* (5), 770.

(4) Hansen, J. A.; Mukhopadhyay, R.; Hansen, J.; Gothelf, K. V. *J. Am. Chem. Soc.* **2006**, *128* (12), 3860.

(5) Liu, G.; Wan, Y.; Gau, V.; Zhang, J.; Wang, L.; Song, S.; Fan, C. *J. Am. Chem. Soc.* **2008**, *130* (21), 6820.

(6) Gooding, J. J. *Electroanalysis* **2002**, *14* (17), 1149.

(7) Wang, J.; Liu, G.; Merkoç i, A. *J. Am. Chem. Soc.* **2003**, *125* (11), 3214.

(8) Wang, J. *Electroanalysis* **2005**, *17* (1), 7.

(9) Drummond, T. G.; Hill, M. G.; Barton, J. K. *Nat. Biotechnol.* **2003**, *21* (10), 1192.

(10) Labib, M.; Khan, N.; Ghobadloo, S. M.; Cheng, J.; Pezacki, J. P.; Berezovski, M. V. *J. Am. Chem. Soc.* **2013**, *135* (8), 3027.

(11) Yu, Y.; Chen, Z.; Shi, L.; Yang, F.; Pan, J.; Zhang, B.; Sun, D. *Anal. Chem.* **2014**, *86* (16), 8200.

(12) Ferguson, B. S.; Buchsbaum, S. F.; Wu, T.-T.; Hsieh, K.; Xiao, Y.; Sun, R.; Soh, H. T. *J. Am. Chem. Soc.* **2011**, *133* (23), 9129.

(13) Pei, H.; Lu, N.; Wen, Y.; Song, S.; Liu, Y.; Yan, H.; Fan, C. *Adv. Mater.* **2010**, *22* (42), 4754.

(14) Das, J.; Cederquist, K. B.; Zaragoza, A. a.; Lee, P. E.; Sargent, E. H.; Kelley, S. O. *Nat. Chem.* **2012**, *4* (8), 642.

(15) Soleymani, L.; Fang, Z.; Sargent, E. H.; Kelley, S. O. *Nat. Nanotechnol.* **2009**, *4* (12), 844.

(16) Soleymani, L.; Fang, Z.; Lam, B.; Bin, X.; Vasilyeva, E.; Ross, A. J.; Sargent, E. H.; Kelley, S. O. *ACS Nano* **2011**, *5* (4), 3360.

(17) Soleymani, L.; Fang, Z.; Sun, X.; Yang, H.; Taft, B. J.; Sargent, E. H.; Kelley, S. O. *Angew. Chem., Int. Ed.* **2009**, *48* (45), 8457.

(18) Bin, X.; Sargent, E. H.; Kelley, S. O. *Anal. Chem.* **2010**, *82* (14), 5928.

(19) Fang, Z.; Soleymani, L.; Pampalakis, G.; Yoshimoto, M.; Squire, J. A.; Sargent, E. H.; Kelley, S. O. *ACS Nano* **2009**, *3* (10), 3207.

(20) Sage, A. T.; Besant, J. D.; Mahmoudian, L.; Poudineh, M.; Bai, X.; Zamel, R.; Hsin, M.; Sargent, E. H.; Cypel, M.; Liu, M.; Keshavjee, S.; Kelley, S. O. *Sci. Adv.* **2015**, *1* (7), e1500417.

(21) Mahshid, S. S.; Camiré, S.; Ricci, F.; Vallée-Bélisle, A. *J. Am. Chem. Soc.* **2015**, *137* (50), 15596.

(22) Xia, F.; Zuo, X.; Yang, R.; White, R. J.; Xiao, Y.; Kang, D.; Gong, X.; Lubin, A. A.; Vallée-Bélisle, A.; Yuen, J. D.; Hsu, B. Y. B.; Plaxco, K. W. *J. Am. Chem. Soc.* **2010**, *132* (25), 8557.

(23) Ricci, F.; Plaxco, K. W. *Microchim. Acta* **2008**, *163* (3−4), 149.

(24) Steel, A. B.; Herne, T. M.; Tarlov, M. J. *Anal. Chem.* **1998**, *70* (22), 4670.

(25) Steichen, M.; Decrem, Y.; Godfroid, E.; Buess-Herman, C. *Biosens. Bioelectron.* **2007**, *22* (9−10), 2237.

(26) Grubb, M.; Wackerbarth, H.; Ulstrup, J. *J. Am. Chem. Soc.* **2006**, *128* (24), 7734.

(27) Liao, W.-C.; Ho, J.-A. A. *Anal. Chem.* **2009**, *81* (7), 2470.

(28) Erdem, A.; Meric, B.; Kerman, K.; Dalbasti, T.; Ozsoz, M. *Electroanalysis* **1999**, *11* (18), 1372.

(29) Xue, D.; Elliott, C. M.; Gong, P.; Grainger, D. W.; Bignozzi, C. A.; Caramori, S. *J. Am. Chem. Soc.* **2007**, *129* (7), 1854.

(30) Das, J.; Lee, J. A.; Yang, H. *Langmuir* **2010**, *26* (9), 6804.

(31) Drummond, T. G.; Hill, M. G.; Barton, J. K. *Nat. Biotechnol.* **2003**, *21* (10), 1192.

(32) Mahshid, S.; Mepham, A. H.; Mahshid, S. S.; Burgess, I. B.; Saberi Safaei, T.; Sargent, E. H.; Kelley, S. O. *J. Phys. Chem. C* **2016**, *120* (37), 21123.

(33) Sage, A. T.; Besant, J. D.; Lam, B.; Sargent, E. H.; Kelley, S. O. *Acc. Chem. Res.* **2014**, *47* (8), 2417.

(34) Das, J.; Cederquist, K. B.; Zaragoza, A. A.; Lee, P. E.; Sargent, E. H.; Kelley, S. O. *Nat. Chem.* **2012**, *4* (8), 642.

(35) Hill, H. D.; Millstone, J. E.; Banholzer, M. J.; Mirkin, C. A. *ACS Nano* **2009**, *3* (2), 418.

(36) Soleymani, L.; Fang, Z.; Lam, B.; Bin, X.; Vasilyeva, E.; Ross, A. J.; Sargent, E. H.; Kelley, S. O. *ACS Nano* **2011**, *5* (4), 3360.

(37) Wong, I. Y.; Melosh, N. A. *Biophys. J.* **2010**, *98* (12), 2954.

(38) Randeria, P. S.; Jones, M. R.; Kohlstedt, K. L.; Banga, R. J.; Olvera de la Cruz, M.; Schatz, G. C.; Mirkin, C. A. *J. Am. Chem. Soc.* **2015**, *137* (10), 3486.

(39) Walter, S. R.; Young, K. L.; Holland, J. G.; Gieseck, R. L.; Mirkin, C. A.; Geiger, F. M. *J. Am. Chem. Soc.* **2013**, *135* (46), 17339.

(40) Springer, T.; Sípová, H.; Vaisocherová, H.; Stepánek, J.; Homola, J. *Nucleic Acids Res.* **2010**, *38* (20), 7343.

(41) Li, T. I. N. G.; Sknepnek, R.; Macfarlane, R. J.; Mirkin, C. A.; Olvera de la Cruz, M. *Nano Lett.* **2012**, *12* (5), 2509.

(42) Okahata, Y.; Kawase, M.; Niikura, K.; Ohtake, F.; Furusawa, H.; Ebara, Y. *Anal. Chem.* **1998**, *70* (7), 1288.

(43) Lapierre, M. A.; O'Keefe, M.; Taft, B. J.; Kelley, S. O. *Anal. Chem.* **2003**, *75* (22), 6327.

(44) Tselepi-Kalouli, E.; Katsaros, N. *J. Inorg. Biochem.* **1989**, *37* (4), 271.

(45) Lee, O.-S.; Schatz, G. C. *J. Phys. Chem. C* **2009**, *113* (6), 2316.

(46) Gong, P.; Levicky, R. *Proc. Natl. Acad. Sci. U. S. A.* **2008**, *105* (14), 5301.

(47) Niwa, O.; Morita, M.; Tabei, H. *Anal. Chem.* **1990**, *62* (5), 447.

DOI: 10.1021/acs.nanolett.6b05153
Nano Lett. XXXX, XXX, XXX−XXX